METHODS AND PROCEDURE FOR THE NONLINEAR DYNAMIC CHARACTERIZATION OF INERTIAL SENSORS UNDER DIVERSE OPERATIONAL CONDITIONS

Leonardo Borges Farconi[(1)] **and Matias Bestard Körner**[(2)]

[(1)]*German Aerospace Center – DLR, Institute of Space Systems, Navigation and Control Systems, Robert-Hooke-Strasse 7, 28359 Bremen, Germany, +49 421-24420-1064, leonardo.borgesfarconi@dlr.de*

[(2)]*German Aerospace Center – DLR, Institute of Space Systems, Navigation and Control Systems, Robert-Hooke-Strasse 7, 28359 Bremen, Germany, +49 421-24420-1260, matias.koerner@dlr.de*

ABSTRACT

Inertial Measurement Units or Navigation Systems (IMU, INS) generally comprise sensors, namely accelerometers and gyroscopes, in many configurations for aerospace Guidance Navigation and Control applications. The sensors are generally modeled and tested for only a few parameters, limiting the behavior knowledge under adverse environmental conditions. Using established and standard testing, such as vibration shaker and rotation table facilities, we developed a methodology to model the nonlinear parameters of sensors, especially those under vibration, high acceleration, and varying thermal conditions. The method records the data in the time domain, establishes the ground truth through sensor fusion, corrects misalignments and identifies ARMAX and NARMAX models using recursive Unified Least Squares (ULS) method. These identification methods are adapted and use a proposed model selection strategy based on the Error Reduction Ratio (ERR), the t-statistic and the Akaike Information Criterion (AIC). The simulation results validate the method's concept and provide insight into the reach of the models derived for accelerometer sensors.

1 INTRODUCTION

Aerospace applications rely on gyroscopes and accelerometers to estimate the current state in space, either embedded in an IMU, INS, or Hybrid Navigation Systems. Specifically, the measurement sensitivity or scale factor, is affected by errors or effects in the readings that degrade the attitude and position estimates with time and finally define the performance of the sensors. Moreover, inertial sensors are characterized in laboratories and modeled to compensate for errors by calibration in the respective navigation filters or to simulate them for performance analysis. However, the sensor models developed will generally reduce the parameters to sensitivity, sensitivity errors (bias), and random white noise. Ideally, some models developed characterize the sensor under different temperature conditions (offset temperature coefficient).

Even though this process may be sufficient for some applications, one crucial question is whether this is improved for applications with more extreme operating conditions, such as Reusable Launch Vehicles (RLV) with lower-grade sensors or Commercial Of-The-Shelf (COTS) based systems. Unfortunately, environmental conditions like vibration, shocks, different temperature ranges cause influences that are usually unknown or, if known, not accounted for in the calibrations. Indeed, the Institute of

Electrical and Electronics Engineers (IEEE) provides some standards and methods for characterizing inertial sensor model parameters and proposes some nonlinear multiple-input models. Nevertheless, the methods are not necessarily inter-correlated, demand too many different tests and analysis, making it difficult for practical applications and usually over-stressing the sensors, besides providing figures not directly related to a time or frequency domain model. On the other hand, previous works that addressed these issues were limited in some sense or did not provide a complete solution to facilitating a complete characterization of inertial sensors, in essence, having limited frequency scopes, limited model orders, prolonged test steps, no consideration of environmental conditions, use of specific equipment usually unavailable in industry, or no consideration for misalignments.
The procedure proposed here uses standard equipment, namely an electrodynamic shaker and rotation table, associated with a particular proposed fixture of easy manufacturing resulting in a single model for different environmental and testing conditions that could be more practical. Finally, the proposed procedure and methods reduce the characterization effort to the same effort employed for usual environmental acceptance or qualification procedures for products in the space industry, especially if embedded in the engineering, acceptance, or qualification tests. Section 2.1 presents the definitions used throughout the paper. Section 2.2 presents an overview of the procedure while the following sections in Section 2 provide more details to the tools and methods that comprise the procedure. Finally, Section 3 explains the simulations performed, presents their results, and discusses their implications.

2 METHODS

2.1 Definitions

The following definitions will be used consistently throughout this text.
Let $F_C = \{\mathbf{n_{ira}}, \mathbf{n_{xra}}, \mathbf{n_{yra}}\}$ be the right-handed orthonormal reference frame located on the sensor case, where IRA, XRA and YRA stand for Input, X and Y Reference Axis, respectively, and $\mathbf{n}$ denotes always a generic normalized frame axis. Let $F_S = \{\mathbf{n_i}, \mathbf{n_p}, \mathbf{n_o}\}$ be the right-handed reference frame located inside the sensor where $\mathbf{n_i}$ is aligned with the sensing axis IA (Input Axis). Let $F_E = \{\mathbf{n_x}, \mathbf{n_y}, \mathbf{n_z}\}$ be an external right-handed reference frame where the inertial quantities, i.e.,rotation rates and accelerations, are known.
The scalar of projections of inertial quantities on the aforementioned axes are represented by the letters a and ω, respectively for acceleration and rotation rate, with the subscript relative to the axis of projection, e.g. a_i, a_{IRA} or a_x for the acceleration on axis $\mathbf{n_i}$, $\mathbf{n_{ira}}$ or $\mathbf{n_x}$, respectively. Consequently $\mathbf{a_C}$, $\mathbf{a_S}$ and $\mathbf{a_F}$ represent the acceleration vectors represented on frames F_C, F_S and F_E respectively, while $\boldsymbol{\omega}_C$, $\boldsymbol{\omega}_S$ and $\boldsymbol{\omega}_F$ represent the rotation rates for the same frames.
The Direction Cosine Matrix (DCM) from F_E to F_S, considering all axes misalignments, is $\mathbf{M_E^S}$, with the first row represented by $\begin{bmatrix}\alpha_{ix} & \alpha_{iy} & \alpha_{iz}\end{bmatrix}$, while the DCM from F_E to F_C is represented by $\mathbf{M_E^C}$, and consequently the DCM from F_S to F_C by $\mathbf{M_S^C} = \mathbf{M_E^C}\left(\mathbf{M_E^S}\right)^{\mathbf{T}}$.

2.2 Characterization procedure

Fig. 1 summarizes the proposed characterization procedure for inertial sensors. The procedure is divided between the test execution and the data analysis. The test execution is thought to be as similar as possible to common characterization and environmental tests performed on space systems, in order to not overtest the sensors and to obtain the necessary nonlinear dynamic characterization without extra specific tests. The inclusion of this procedure on a system level is, however, out of the scope of this text.
Block 1 of Fig. 1 represents common characterization procedures performed for accelerometers and gyroscopes on a rotation table. For accelerometers the Static Multipoint Test can be used. For gyro-

scopes, the Gyro Scale Factor Test Series, which means rotation at different rates and around at least two different axes, provide the necessary excitation. For both cases, data shall be acquired on the time domain without any averaging. To also observe noise components, one can stop the rotation table, for long enough periods of time, at specific orientations in the middle of the aforementioned tests without dismounting the sensors.
The tests performed on the shaker, also referred here as vibration table and represented by blocks 2, 3 and 4, can be varied and can include not only random vibration profiles, but also shocks and sine excitation, for example.
During all these test cases, temperature can be varied to also include this factor in the model or understand the sensitivity of some parameters to it. The details of this specific case won't be treated with attention in this text.
The core of the whole procedure lies on a simple concept: to remove all sensor and fixture misalignments from the reference test data and bring them all to a same reference frame, i.e. F_S, on which a batch parameter identification can be performed with all the necessary excitation to estimate nonlinear and dynamic parameters in an unified model. For this to be possible, some special care is necessary on the identification methods, the fixture and the data acquisition setup, and the excitation profiles, addressed on sections 2.5, 2.6, 2.7, 2.3 and 3.2, respectively.
This concept is represented on the Data Analysis section of Fig. 1. In blocks 5 and 6, the algorithm explained on 2.7.1 is responsible for finding the best nonlinear dynamic model - also referred here simply as the complex model - that fits to the provided data and estimate the misalignment $\mathbf{M_E^S}$ for that specific test case. Independently of whether the final goal is to use a more complex model or just a simplified model with only scale and bias, this step needs to be performed with the complex model in order to remove biases that can be introduced in the misalignment estimation due to higher order or dynamic effects from the sensor.
Since the main sensing quantity for gyroscopes is the rotation rate, and specifically for fiber-optic rate gyros the sensitivity to vibrations may not be necessarily linked to a specific sensor reference frame, block 6 cannot be performed for gyroscopes. Moreover, it is desired the vibration sensitivity to be also represented on the same frame F_S as the rotation rate sensitivity. In this case, the sensor case alignment $\mathbf{M_E^C}$ for these tests should be known to very high accuracy and the test misalignment $\mathbf{M_E^S}$ should be obtained by making $\mathbf{M_E^S} = \mathbf{M_C^S M_E^C}$, where $\mathbf{M_C^S}$ is estimated from block 5.
Blocks 7 and 8 use the test misalignments $\mathbf{M_E^S}$ obtained in previous blocks to transform all reference inertial quantities to the same frame F_S. In block 9, these test data are then concatenated in order to run a batch identification where no misalignment estimation is needed. When just a simple model is needed,e.g. to be used on simple calibrations running on inertial navigation systems, one can use the identification algorithm explained on Section 2.6 fixed on the desired model, as represented by block 10. On the other hand, with block 11, explained on Section 2.7.2, it is possible to obtain the aforementioned complex model to be used in simulations or simply to deeply understand the behaviour of the sensor under test in the test conditions.

2.3 The vibration fixture and setup

The first part of the characterization procedure focuses on test execution providing the raw data from the sensors in a relevant vibration environment. In this case, the vibration source is an electrodynamic shaker with a so-called slip table providing a perpendicular vibration motion against the gravity vector, commonly used in structural tests for aerospace systems and components. Additionally, the mounting fixture interfacing the sensors with the shaker integrates the thermal system, also called the temperature-controlled mounting fixture. When it comes to data acquisition, the procedure proposed on Section 2.2 relies on a time domain regression, which means that the time domain reference acceleration of the mounting fixture needs to be known with accuracy. The exact details of this setup

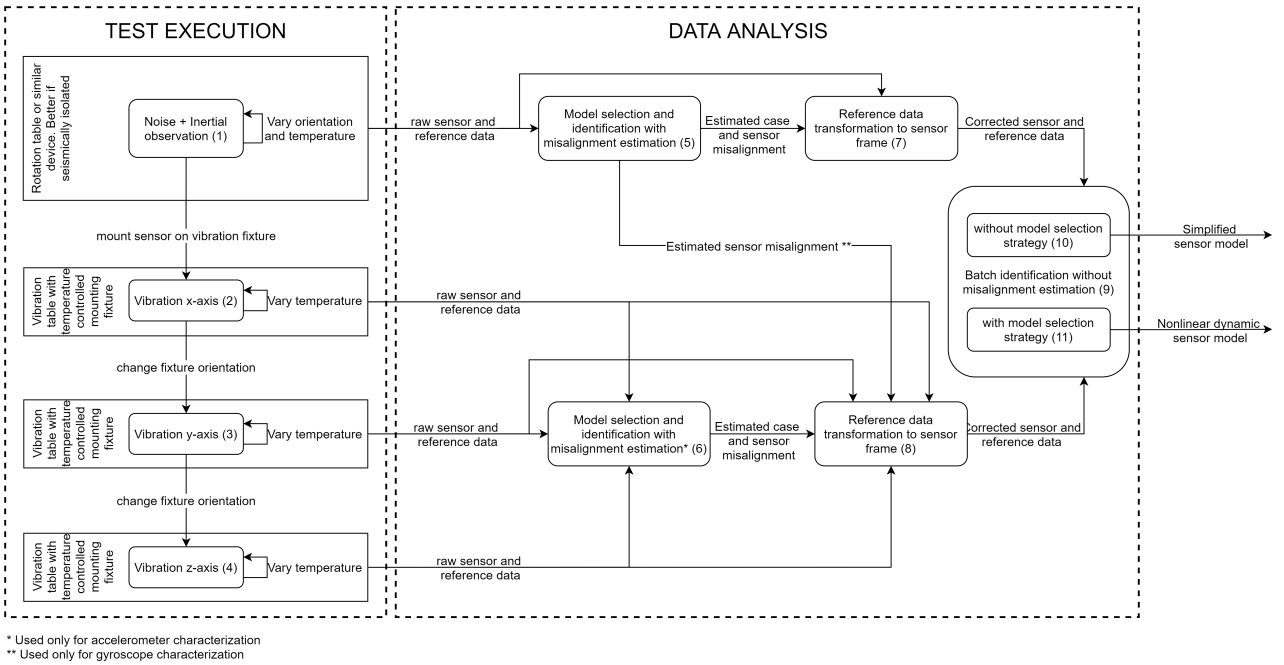

Figure 1: Proposed inertial sensor characterization procedure. Source: Created by the Author.

will not be clarified here, but the proposal is to use a sensor fusion between reference accelerometers mounted on the fixture and reference linear encoders sensing the shaker displacement.

Since the fixture will include the sensors under test and additional monitoring sensors, the fixture's influence must be minimal such that all sensors test against the same vibration profile in frequency and phase. The material and geometry should reduce any resonance effects the fixture may create on the sensors under test and interface all items as rigidly as possible with the vibration table.

Furthermore, the fixture contains slots responsible for holding the accelerometers under test and providing adequate sensor orientation against the vibration axis. In the case of the accelerometers, the fixture shall provide at least three orientations for testing one sensor as indicated per IA, Pendulous Axis (PA), and Output Axis (OA) in Fig. 2. The angle α may be any angle different from $0\,\mathrm{deg}$, but the suggestion is to make $\alpha = 25\,\mathrm{deg}$. These orientations guarantee that one sensor will be sufficiently excited in all directions to provide observability for all sensor parameters and misalignment. For the misalignment between sensor case and fixture to be estimated, however, it shall be fixed for all tests using the fixture, even if not known or not close to zero. For this to be valid, assuming that the reference accelerations are known for the fixture reference frame, independently of fixture misalignment in relation to the shaker, the sensor shall be mounted only once on the fixture and the fixture remounted on the shaker to provide the desired test orientation. Fig. 3 provides an example of such a fixture for testing 3 accelerometers at the same time.

Similar slots provide the same functionality as the accelerometer slots but for the gyroscopes. The difference here is that these slots shall place the three gyroscope axes parallel to the vibration axis for each of the three possible configurations; in other words, $\alpha = 0\,\mathrm{deg}$. This alignment shall be manufactured and known as accurately as possible in relation to the reference frame. In this case, the fixture may remain fixed and the sensors swapped in between the slots for the different tests. Fig. 4 gives an example of such a fixture for testing 4 gyroscopes at the same time.

Additional slots hold the monitoring accelerometers. The skewed orientations ensure that no monitoring sensor shall be placed in the same orientation as another monitoring sensor, increasing the observability of the setup. For example, one could place four single-axis sensors orientated in a 45°

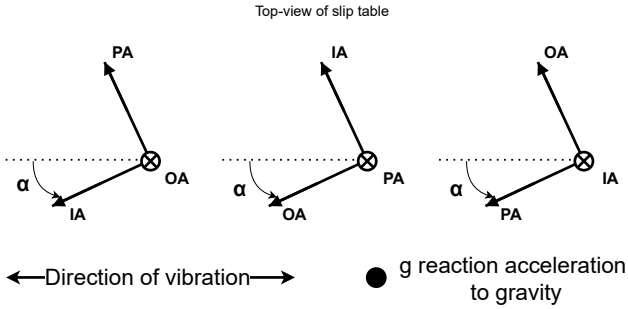

Figure 2: Accelerometer slots orientations. Source: Created by the Author.

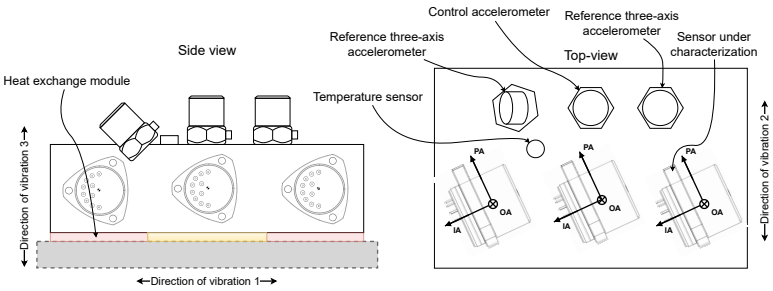

Figure 3: Mounting fixture example for 3 accelerometers. Source: Created by the Author. Sensor sketches adapted from "AI-Q-20X0 Accelerometers User Manual, Rev 1.0 22/09/2015, INNALABS".

cone configuration; or two three-axis sensors skewed 45° of each other, spread around the mounting fixture to obtain readings close to all sensors under test.
Furthermore, the shaker hardware requires control accelerometers for which additional slots exist, mounted rigidly and reliably aligned with the vibration axis, preferably as close as possible to all sensors under test.
The heat exchange module may be any device capable of forcing heat exchange between the mounting fixture and the vibration slip table, which is a thermal sink. Specifically, a thermoelectric module, commonly known as Peltier module, can exchange heat between the fixture and the shaker slip table. Moreover, a thermal isolation also supports the fixture where the thermoelectric module does not provide the thermals-mechanical interface. Finally, the thermal controller gets the fixture reference temperature from temperature sensors.

2.4 Characterization models

As previously discussed, in order to perform the proposed procedure on Section 2.2 it is necessary to use a model that can capture the most important effects on the sensor output so as to not let unmodelled effects to include biases in the misalignment estimations. Sections 2.4.1 and 2.4.2 present nonlinear and dynamic models for accelerometers and rate gyroscopes, respectively, which can capture most of these effects.

2.4.1 Accelerometers

According to [1, § 8.3], the model equation of the accelerometer is defined as a static model dependent on the components of applied acceleration, angular velocity, and angular acceleration. The same standard, however, states that these model parameters can be influenced by frequency depending

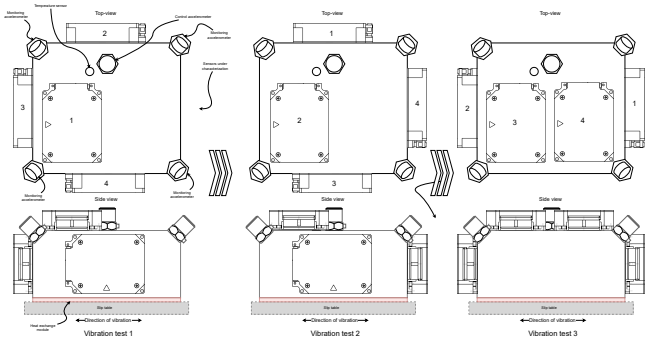

Figure 4: Mounting fixture example for 4 gyroscopes. Source: Created by the Author. Sensor sketches adapted from "µFORS-3U User Manual, Revision B, Northrop Grumman LITEF GmbH".

on the accelerometer type. That influence can be analyzed by using the method *5.3.21 Frequency Response* from [1]. If the frequency dependency is found to be high, however, there is no way of considering this information in the static model if not by assuming a model error. A dynamic model, on the other hand, can incorporate the frequency response characteristics of the system if this is found to be of importance. It is possible also to model colored system noise which is the case for some accelerometers.

Pendulous accelerometers are subject to crosscoupling and vibropendulous rectification caused by an inherent rotation of the IA as a function of input acceleration. These parameters become more important when accelerations in IA and PA are vibratory, which is the case for aerospace and military INS. It may also be the case that, according to [1], this effect of vibropendulous rectification vary dramatically with frequency, which can then be modeled by a dynamic model.

Parameters related to angular velocities and accelerations , without loss of generality, not considered here.

Considering all the mentioned effects above, let $\mathbf{u_{ES}(k)} \in \mathbb{R}^{\mathbf{12}}$ be a known input at instant $k \in \mathbb{Z}$ composed of accelerations in both frames F_E and F_S and represented by Eq. 1.

$$\mathbf{u_{ES}(k)} = \begin{bmatrix} a_x(k) & a_y(k) & a_z(k) & {a_i}^2(k) & {a_p}^2(k) & {a_o}^2(k) & a_i(k)a_p(k) & a_i(k)a_o(k) & a_p(k)a_o(k) \\ sign(a_i(k)) & |a_i(k)| & a_i(k)|a_i(k)| \end{bmatrix}^T \tag{1}$$

If the noise $v(k)$ was known, the optimal generalized ARMAX estimator for a dynamic representation of a pendulous accelerometer in frames F_E and F_S could be represented by Eq. 2.

$$\begin{aligned} \hat{y}_{ES}(k|k) =& K_b + \mathbf{b_0^T u_{ES}(k)} + \ldots + \mathbf{b_m^T u_{ES}(k-r)} + \\ &+ a_1 y(k-1) + \ldots + a_r y(k-r) + c_1 v(k-1) + \ldots + c_r v(k-r) + v(k) \end{aligned} \tag{2}$$

where r is the model order, and $\mathbf{b_0^T}, ..., \mathbf{b_r^T}$, $a_1, ..., a_r$ and $c_1, ..., c_r$ are real coefficients. Similarly, for $\mathbf{u_S(k)} \in \mathbb{R}^{\mathbf{10}}$ in F_S, represented by Eq. 3, the estimator could be represented by Eq. 4.

$$\mathbf{u_S(k)} = \begin{bmatrix} a_i(k) & {a_i}^2(k) & {a_p}^2(k) & {a_o}^2(k) & a_i(k)a_p(k) & a_i(k)a_o(k) & a_p(k)a_o(k) \\ sign(a_i(k)) & |a_i(k)| & a_i(k)|a_i(k)| \end{bmatrix}^T \tag{3}$$

$$\begin{aligned} \hat{y}_{S}(k|k) =& K_b + \mathbf{b_0^T u_S(k)} + \ldots + \mathbf{b_m^T u_S(k-r)} + \\ &+ a_1 y(k-1) + \ldots + a_r y(k-r) + c_1 v(k-1) + \ldots + c_r v(k-r) + v(k) \end{aligned} \tag{4}$$

Please note that the choice of Eqs. 1 and 3 does not reduce the generality of the proposal.

2.4.2 Gyroscopes

Reference [2] presents a dynamical model dependent on the components of rotations, temperature, and drift errors. The models proposed on this chapter are a combination of the standard and other references on literature.
The IEEE standard presents a model that is both deterministic and stochastic. The deterministic part is related to the rotation rate, temperature and environmental sensitivities and deterministic errors; while the stochastic part can be summarized as colored noise.
Annex B on [2] discusses different methods for modeling the behavior of a gyroscope, citing that there is no need to model the deterministic sensor behavior as a dynamical system for a 1-axis gyroscope. The stochastic part, though, is inherently dynamic.
The colored noise on gyros is very concerning for INSs. It is usually modeled and removed from the sensor readings as seen on [3], [4], [5], [6], [7], where colored noise is either modeled in state-space models and removed with filters of appropriate order, or simply removed using adaptive or FIR filters.
All gyroscopes are to some extent, including Fiber-optic gyroscopes (FOGs), sensitive to vibrations. Those add undesired noise and consequently errors to INSs. Reference [8] shows that the vibration error can be modeled as an additive noise, while [9] presents a much more elaborated model of the vibration influence on the FOG output with results similar to what was observed in [10]. In summary, the vibration induced error on the rate output can be modeled additive to the output and linearly dependent to the input acceleration amplitude and frequency.
Considering all the mentioned effects, the FOG can be modeled by Eq. 5 when considering inputs simultaneously at frames F_E and F_S, and by Eq. 6 when considering only frame F_S. In both, $\Omega(k)$ denotes the sensor output at the instant k, $v(k)$ denotes a random white noise, $A(q)$ and $B(q)$ are polynomials of order 3, $C(q)$ to $H(q)$ are polynomials of order 2, and q denotes the forward shift operator in time domain, i.e., $q^{-1}x(k) = x(k-1)$.

$$\Omega_S(k)S_0\left[1+10^{-6}\varepsilon_T T(k)+c_{f1}\omega_i(k)\right] = c_x\omega_x(k)+c_y\omega_y(k)+c_z\omega_z(k)+c_{T1}T(k)+c_{T2}T(k-1)+ \\ +\frac{B(q)}{A(q)}n'_\Omega(k)+\frac{D(q)}{C(q)}a_i(k)+\frac{F(q)}{E(q)}a_p(k)+\frac{H(q)}{G(q)}a_o(k)+D_F \tag{5}$$

$$\Omega_{ES}(k)S_0\left[1+10^{-6}\varepsilon_T T(k)+c_{f1}\omega_i(k)\right] = c_i\omega_i(k)+c_{T1}T(k)+c_{T2}T(k-1)+ \\ +\frac{B(q)}{A(q)}n'_\Omega(k)+\frac{D(q)}{C(q)}a_i(k)+\frac{F(q)}{E(q)}a_p(k)+\frac{H(q)}{G(q)}a_o(k)+D_F \tag{6}$$

2.5 Misalignment estimation

The sensor misalignments $\mathbf{M_C^S}$ During the test executions of Fig. 1 are unknown. If one decides to live with the errors, it could be assumed as an identity transformation, where $\mathbf{n_i}$ is exactly $\mathbf{n_{ira}}$. The transformation from F_E to F_C, on the other hand, is known. However, in any test fixture there are misalignment errors that add uncertainties to this transformation matrix $\mathbf{M_E^C}$. If those uncertainties are well controlled and maintained low, one may choose to ignore them, including them in the sensor parameter estimation uncertainties. If better accuracy is necessary, however, for one same fixture one should always perform the test at least twice: in the regular position and in the opposite direction. This will likely cancel or reduce the fixture errors in the parameter estimation. Even though this last option seems to be a solution to the fixture problem, two issues have to be considered:

- The number of tests increases to guarantee that positions are tested in both ways, and
- depending on the fixture, it may not be trivial to test the sensor in the opposite direction for all test cases.

Having said this, the proposition here is to estimate the fixtures' misalignment along with the sensor misalignment, giving the necessary conditions for Block 9 in Fig. 1, as already explained.
With this purpose in mind, for an inertial sensor parameter identification on F_E, it is always possible to identify three parameters θ_x, θ_y and θ_z which are respectively the projection of the sensing axis on the axis of F_E, as exemplified on Eq. 7 for an acceleration case.

$$\theta_i a_i = \theta_i(\alpha_{ix}a_x + \alpha_{iy}a_y + \alpha_{iz}a_z) = \theta_x a_x + \theta_y a_y + \theta_z a_z \tag{7}$$

From these parameters, the exact orientation of $\mathbf{n_i}$ can be obtained. There are, however, infinite possibilities for the directions of $\mathbf{n_p}$ and $\mathbf{n_o}$, and even though they would regularly not be important, here it is important to keep their choice consistent in order to have a proper final batch identification. For this reason, the proposed approach here is to simply rotate the whole F_C around the normal vector from the cross product between $\mathbf{n_{IRA}}$ and $\mathbf{n_i}$. This is summarized in Algorithm 1, where $\hat{\theta}_i$, $\hat{\theta}_x$, $\hat{\theta}_y$ and $\hat{\theta}_z$ refer to the estimated main sensitivities for an inertial quantity and $\mathbf{M_E^C}$ refers to the nominal expected sensor case misalignment.

Algorithm 1 Misalignment axes calculation

$\hat{\theta}_i \leftarrow \sqrt{\hat{\theta}_x^2 + \hat{\theta}_y^2 + \hat{\theta}_z^2}$
$\hat{\alpha}_{ix} \leftarrow \hat{\theta}_x / \hat{\theta}_i$
$\hat{\alpha}_{iy} \leftarrow \hat{\theta}_y / \hat{\theta}_i$
$\hat{\alpha}_{iz} \leftarrow \hat{\theta}_z / \hat{\theta}_i$
$\hat{\mathbf{n}}_i \leftarrow \begin{bmatrix}\hat{\alpha}_{ix} & \hat{\alpha}_{iy} & \hat{\alpha}_{iz}\end{bmatrix}^T$
$\mathbf{n_{IRA}} \leftarrow \left(\begin{bmatrix}1 & 0 & 0\end{bmatrix} \mathbf{M_E^C}\right)^{\mathbf{T}}$
$\hat{\mathbf{n}}_R \leftarrow \mathbf{n_{IRA}} \times \hat{\mathbf{n}}_\mathbf{i}$
$\delta_R \leftarrow acos(\mathbf{n_{IRA}} \bullet \hat{\mathbf{n}}_\mathbf{i})$
$\mathbf{R}(\hat{\mathbf{n}}_\mathbf{R}, \delta_\mathbf{R}) \leftarrow$ rotation matrix relative to the rotation of δ_R angle around the $\hat{\mathbf{n}}_R$ axis.
$\hat{\mathbf{n}}_p = \mathbf{R^T}(\hat{\mathbf{n}}_\mathbf{R}, \delta_\mathbf{R}) \left(\begin{bmatrix}0 & 1 & 0\end{bmatrix} \mathbf{M_E^C}\right)^{\mathbf{T}}$
$\hat{\mathbf{n}}_o = \mathbf{R^T}(\hat{\mathbf{n}}_\mathbf{R}, \delta_\mathbf{R}) \left(\begin{bmatrix}0 & 0 & 1\end{bmatrix} \mathbf{M_E^C}\right)^{\mathbf{T}}$
$\mathbf{M_E^S} \leftarrow \begin{bmatrix}\hat{\mathbf{n}}_i & \hat{\mathbf{n}}_p & \hat{\mathbf{n}}_o\end{bmatrix}^{\mathbf{T}}$

2.6 Parameter identification method

The model on Section 2.4.2 is evidently a complex NARMAX model which, without proper arrangement, cannot be unbiasedly characterized. There is, however, a solution for estimating the parameters of such types of model. Reference [11] proposes to rewrite the model to make it linear in the parameters. After this a modified Extended Least-Squares algorithm can be applied to obtain an unbiased estimation of the model parameters. This is called by [11] the Rational Model Estimator (RME). Reference [12], on the other hand, extends the presented on [11] to a *Generalized NARMAX model* and a *Unified Least-Squares Algorithm* (ULS) which can also be used for the models on Section 2.4.1. The details of the ULS will not be clarified here and we encourage the reader to look into the references for more information.

2.7 Model selection strategy

In order to have an unbiased parameter identification on Section 2.2, the models proposed on Section 2.4 have many regressors. This may not be necessary for every sensor and may also decrease model

accuracy, as indicated by [13] which states that if the model order is way larger than the necessary, the model estimation may be ill-conditioned. Another point of attention brought by [13] is the *Bias-Variance Dilemma* first introduced by [14], which means in summary that there is an optimal number of parameters, not necessarily large, that causes the minimum modeling error. Considering this, a model fitness metric shall be established to help tailor the model in regards to its terms and finally decide which model from all the options ranks better to be used in further applications. Three metrics are proposed to be used in this tailoring process: the Error Reduction Ratio (ERR), the *t-statistic* and the Akaike Information Criterion (AIC).

The ERR is a parameter ranking metric that quantifies the contribution of each model parameter for the system output. This means that a parameter with higher ERR will be more important than another parameter with a lower ERR. The ERR for a parameter j is

$$[ERR]_j = \hat{g}_j^2 \frac{\mathbf{q}_j^T \mathbf{q}_j}{\mathbf{Y}^T \mathbf{Y}} \tag{8}$$

where $\hat{\mathbf{g}} = [\hat{g}_1, ..., \hat{g}_p] = (Q^T Q)^{-1} Q^T \mathbf{Y}$, $Q = [\mathbf{q}_1, ..., \mathbf{q}_p]$, $\mathbf{\Phi} = QR$ and QR is the QR decomposition of the regression matrix Φ, where R is upper-diagonal with zeros in the main diagonal, Q is made of orthogonal columns $\mathbf{q}_j$, and $Q^T Q = D$ where D is diagonal.

The AIC is a model ranking metric that tries to tackle the *Bias-Variance Dilemma* by accounting for the error variance but penalizing the inclusion of more parameters. In this sense, a model with a lower AIC should be statistically better than a model with a higher AIC. Therefore,

$$AIC(n_\theta) = N ln\left[\sigma_e^2(p)\right] + 2p \tag{9}$$

where N is the number of data, p its the number of model parameters, and $\sigma_e^2(p)$ is the residuals variance over the identification data for the model with p parameters ranked accordingly. Let AIC_{min} be the minimum AIC between all the model AICs. The relative likelihood that a model minimizes the information loss can be obtained by Eq. 10.

$$p_{AIC}(n_\theta) = exp\left((AIC_{min} - AIC(n_\theta))/2\right) \tag{10}$$

The *t-statistic* is useful to statistically remove unnecessary parameters. If a parameter has influence on the model output, its value should be statistically different from zero, otherwise one can simplify the model by removing this parameter. Assuming that $\hat{\mathbf{\Theta}}$ is normally distributed and with covariance $\sum_{\hat{\Theta}}$ as previously calculated, one can use Student's t-test for testing the null hypothesis that $\hat{\theta}_j = 0$ for $j = 1, ..., p$. The t-statistic for this hypothesis is

$$t_j = \frac{\hat{\theta}_j}{\sqrt{\Sigma_{\hat{\Theta},j}}} \sim t(N - p - 1) \tag{11}$$

where $\Sigma_{\hat{\Theta},j}$ is the j-th element on the diagonal of $\Sigma_{\hat{\Theta}}$. Using t_j in the two-sided cumulative Student's t distribution with $N - p - 1$ degrees of freedom, it is possible to obtain the confidence level necessary for the null hypothesis $(\hat{\theta}_j = 0)$ to be rejected.

For each model it is also important to check whether the model regression generated residuals of mean zero, which otherwise would mean a biased estimation. For this, the same *t-test* can be performed on each model residuals to check the probability $p_{res}(n_\theta)$ at a defined confidence interval that this model residuals are zero. Finally. the fitness of the model with n_θ parameters can be obtained by making $fitness(n_\theta) = p_{res}(n_\theta) p_{AIC}(n_\theta)$.

2.7.1 Model selection with misalignment estimation

Algorithm 2 summarizes the model selection strategy with misalignment estimation, where $\hat{\mathbf{\Theta}}^{ES}$ is the vector of estimated parameters θ_j^{ES} for a model on frames F_E and F_S being identified, while $\hat{\mathbf{\Theta}}^{S}$ is the vector of estimated parameters θ_j^{S} for a model on frame F_S.

Algorithm 2 Model Selection Strategy for isolated tests considering misalignment estimation

1: Estimate the sensor parameters $\hat{\mathbf{\Theta}}^{ES}$ using the ULS from Section 2.6 and model 2 for accelerometers, or 5 for gyros.
2: Rank the sensor parameters $\hat{\theta}_j^{ES}$ using the ERR (Eq. 8) with the regression matrix $\mathbf{\Phi}^{ES}$ from the previous step.
3: **for** all j ranked in decrescent order based on $[ERR]_j$ **do**
4: Modify the model to contain only the regressors related to parameters $\hat{\theta}_1^{ES}, ..., \hat{\theta}_j^{ES}$.
5: Estimate again the sensor parameters $\hat{\mathbf{\Theta}}^{ES}$ from 1 to j using the ULS from Section 2.6 and model 2 for accelerometers, or 5 for gyros.
6: Estimate the test misaligment $\mathbf{M_E^S}$ using the method proposed on Section 2.5.
7: Modify the model 4 for accelerometers, or 6 for gyros, to remove parameters that are not related to the selected parameters $\hat{\theta}_1^{ES}, ..., \hat{\theta}_j^{ES}$.
8: Estimate the sensor parameters $\hat{\mathbf{\Theta}}^{S}$ using the ULS from Section 2.6 and the modified models 4 or 6 from previous step.
9: Remove spurious parameters using Student's t-test from Section 2.7 and the regression matrix $\mathbf{\Phi}^{S}$ from previous step, and update the model.
10: Estimate again the remaining sensor parameters using the ULS from Section 2.6 and the modified models 4 or 6 from previous step.
11: Calculate $AIC(n_\theta)$ for this model using Eq. 9.
12: Calculate $p_{res}(n_\theta)$ for this model using Student's t-test from Section 2.7
13: **end for**
14: Calculate the relative likelihood $p_{AIC}(n_\theta)$ for each model and subsequently their respective $fitness(n_\theta)$, as proposed on Section 2.7.
15: Select best model and its test misalignment $\mathbf{M_E^S}$ based on the highest $fitness(n_\theta)$.

2.7.2 Model selection without misalignment estimation

The model selection strategy when no misalignment estimation is necessary is similar to the one proposed in Algorithm 2. The difference is that steps 6, 7 and 8 do not exist, and the data used should be in frame F_S, in order to obtain the parameters $\hat{\mathbf{\Theta}}^{S}$ instead of $\hat{\mathbf{\Theta}}^{ES}$.

3 RESULTS AND DISCUSSION

Due to the ongoing development of the proposed work only a simulation based verification was done to provide a first insight into the methodology. The goal here is to compare three cases: (1) An accelerometer characterization based only on a rotation table test and a sensitivity and sensitivity error (bias) sensor model; (2) An accelerometer characterization based on both rotation table and shaker tests using the procedure from Section 2.2 with sensors models from Eqs. 2 and 4 for misalignment estimation but the same sensor model as (1) for the batch characterization of block 9 in Fig. 1; and (3) the same process as 2 but with the same models from Eqs. 2 and 4 for the batch characterization. To

keep this analysis simple, models 2 and 4 will be kept with $r = 0$ (static model), and the gyroscope models and the Model Selection from Section 2.7 will not be considered. For cases (2) and (3), the same procedure of misalignment estimation was done with the simple model of case (1) just to show the advantages of using a more complete model.

3.1 Simulation Model Based Verification Method

Eq. 12 was modeled in simulink to represent the accelerometer under test, where $\mathbf{a_S} = \mathbf{R_{OA}}(\alpha_\mathbf{o})\mathbf{R_{PA}}(\alpha_\mathbf{p})\mathbf{a_C}$. $\mathbf{a_S}$ and $\mathbf{a_C}$ follow the same definition as previously; α_p and α_o are misalignment angles around PA and OA, respectively; R_{PA} and R_{OA} are DCMs of rotation around PA and OA, respectively; $K_{ii}(s)$, $K_{pp}(s)$ and $K_{oo}(s)$ are first-order high-pass filters of gain K_{ii}, K_{pp} and K_{oo}, and bandwidth bK_{ii}, bK_{pp} and bK_{oo}, respectively; ε_N, ε_B and ε_K are random white, pink and brown noises of parameters N, B and K, respectively.

$$\begin{aligned} y =& K_i \left(K_b + a_i + K_s sign(a_i) + K_a|a_i| + K_{oq}a_i|a_i| + K_{ip}a_i a_p + K_{io}a_i a_o + K_{po}a_p a_o + \right. \\ &\left. + K_{ii}(s)a_i^2 + K_{pp}(s)a_p^2 + K_{oo}(s)a_o^2 + \varepsilon_N + \varepsilon_B + \varepsilon_K \right) \end{aligned} \tag{12}$$

Fig. 5 presents the input data and the simulated sensor response for the rotation table test. Before being used in the simulation, the input data is transformed to add the extra case misalignment, which is assumed unknown by the subsequent regression algorithm. Here, the simulated case misalignment is a 2° rotation around the sensor case Y axis. The test profile is comprised of 3 rotations around each sensor case axis and a rotation around the axis [1,1,1].

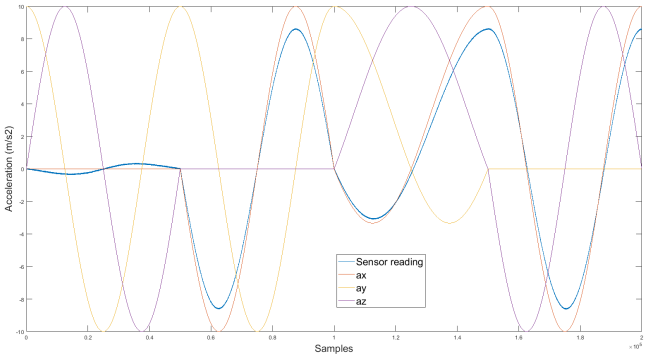

Figure 5: Rotation table simulation input and output data. Source: Created by the Author.

Fig. 6 presents the input data and the simulated sensor response for the vibration test. Similarly here, case misalignment is simulated and in this case it is a 2° rotation around the axis [1,1,1] of the sensor case. The test profile is comprised of 3 different orientations according to Fig. 2. At each orientation, the excitation is comprised of 1 second without vibration, 1 second with a 10 Hz 30g sine, and 1.5 seconds of random vibration of around 17 gRMS. The three images in Fig. 6 are the same test, separated only for visualization purposes.
Table 1 shows the parameters used for simulating the accelerometer model.

Table 1: Accelerometer model parameters

K_i	K_b	α_o,α_p	K_{ii},K_{pp},K_{oo}	bK_{ii},bK_{pp},bK_{oo}	K_{ip},K_{io},K_{po}	N	B	K
0.86	4e-3	1.4e-3	60e-6	500	1e-3	1e-4	1.5e-3	0

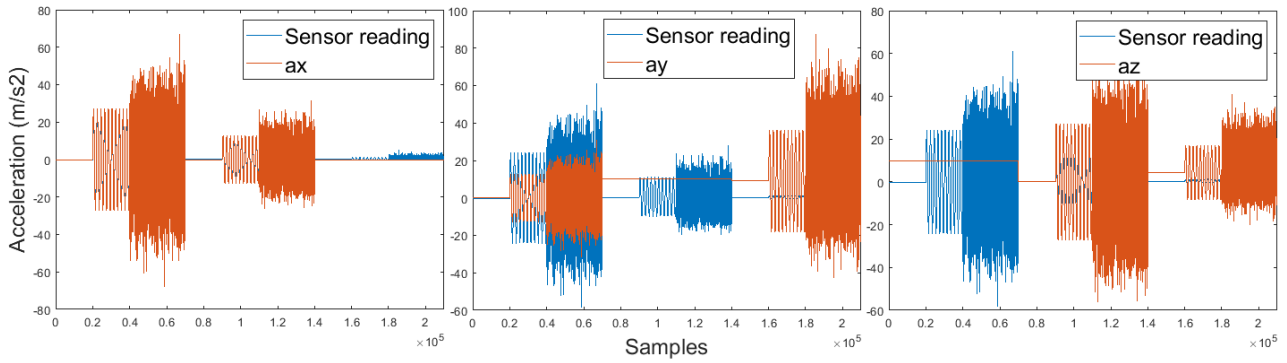

Figure 6: Shaker simulation input and output data. Source: Created by the Author.

For verifying the results, after the respective model identifications for each test case as described above and using the procedure from Section 2.2, the same original test data on frame F_E was transformed to frame F_S but using the real misalignments $\mathbf{M_E^S}$ instead of the estimated ones. This data was then fed to the identified models and their sensor output result compared with the output from the simulink model to observe the error.

3.2 Comments on profiles and regression models

In any case of model identification, the choice of the excitation profiles and the regression models is crucial to the success of the identification. The profiles need to be chosen in order to excite all the parameters to be identified. In some cases this is not completely possible and, therefore, one may need to adjust the regression model in order not to have wrong results. This is the case of the rotation table test, as pointed out by [1, § 12.3.5.7], which cites that parameters related to a_p^2 and a_o^2 cannot be estimated simultaneously with K_b and parameters related with a_i^2. Therefore the model in Block 5 of Fig. 1 needs to be adapted to remove a_p^2 and a_o^2 related parameters from the estimation.
The shaker orientation is also an issue when exciting PA and OA in the third configuration of Fig. 2. Here, if one decides to use a vertical shaker to facilitate testing and the design of the fixture, making IA close to zero, the results are degraded. Moreover, as pointed out by [1, § 12.3.5.7], the sensor bias cannot be estimated in this test, otherwise it corrupts the other parameter estimations.
Lastly, as also pointed out by [1, § 12.3.5.7], the parameters related to $sign(a_i)$, $|a_i|$ and $a_i|a_i|$ should not be included in the identification if they are not statistically significant because they degrade the identification of the bias, scale factor and misalignment. For this simulation they were assumed to be zero and will be studied in more detail in the future.

3.3 Simulation Results

The first row of Table 3 shows the error in angles between the real and the estimated sensor and sensor case misalignment for the rotation table and shaker tests. The second row shows the same errors if a simple scale and bias model was used for estimating the misalignment instead of a more complete model.

Table 2: Misalignment estimation error (in degrees)

Model used	Rotation table	Shaker
Simple	0.0089	0.7768
Complete	0.0043	0.0130

Table 3 shows the parameters estimated for each regressor for the respective model. Regressor 1 means the sensor bias. Table 4 shows the verification error variance for each model resulting from each test case. Fig. 7 shows the errors for each test case.

Table 3: Estimated parameters for each regressor and test case

Test case	a_i	a_i^2	a_p^2	a_o^2	a_{ip}	a_{io}	a_{po}	1
1	0.860	-	-	-	-	-	-	3.81e-3
2	0.868	-	-	-	-	-	-	63.04e-3
3	0.864	3.37e-5	-9.14e-6	5.80e-5	8.30e-4	8.94e-4	8.81e-4	0.26e-3

Table 4: Verification error variance (in m/s2)

Test case 1	Test case 2	Test case 3
300e-4	257e-4	3e-4

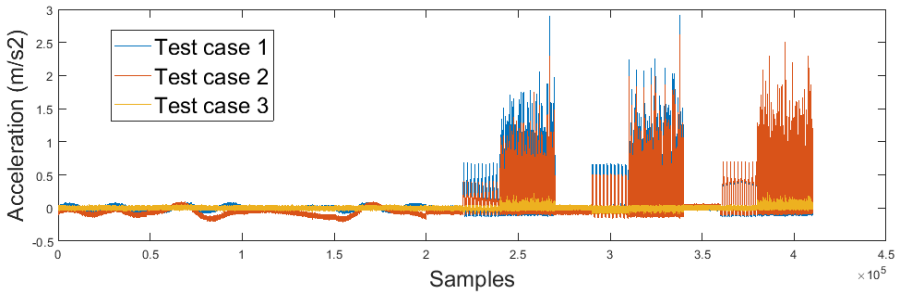

Figure 7: Verification errors for batch estimation. Source: Created by the Author.

3.4 Results Evaluation and Discussion

The K_p and K_o used for the simulation represent a sensor misalignment angle of around $0.12°$. With the previously presented sensor case misalignments, this adds up to $2.08°$ for the rotation table test and $2.94°$ for the shaker test. Table 3 shows that the procedure of Section 2.2, even in the presence of big misalignments, is viable by giving errors in the order of only 0.4% of the overall misalignment and 10% of the sensor misalignment in the worst case scenario of vibration, besides an error of only 0.2% and 3.75% for the rotation table test in relation to the overall misalignment and sensor misalignment, respectively. One possible reason for this error of 10% are the unmodeled dynamic effects not considered here since the model selection with higher order terms was not used for this simulation. In both cases, however, a simple model proved to be not usable for this procedure.
Table 4 shows that the verification error variance degrades from test case 1 to case 3, with a drastic decrease on test case 3. This implies that the proposed procedure provides a model that gives a better approximation of the real sensor on average, when considering different operational conditions. Fig. 7, however, shows an expected negative side effect. This is a larger error for the model of test case (2) for the the less dynamic operational condition, even though it showed lower error for the overall profile. Despite this, the usage of this procedure to have a simple model characterized against different operational conditions presents to be as a more accurate alternative for dynamic demanding missions considering that one can tailor it to the necessary mission conditions: Based on a mission analysis and on the accuracy of each setup, the batch regression can be done with different weights for the

different operational conditions and verified with mission representative simulations, where one can evaluate whether dynamic conditions are more present than static ones, to find the model of lowest error for the mission.
Moreover, The usage of this procedure with the proposed test fixture for obtaining nonlinear models is clearly possible from the good results of test case (3) compared to the other 2 test cases. Whether this procedure is more accurate than the existing list of procedures and methods presented on [1, § 12] is yet to be verified. Its reduced complexity of only 4 tests, however, compared to dozens of tests from [1, § 12] to obtain the same parameters proves already to be a good advantage both in terms of test time and effort, as also stress imposed on the sensor under test. Besides that, it is expected that by considering the dynamic effects and colored noise with the model selection strategy, not tested here, the accuracy can be further improved.

4 CONCLUSION AND FUTURE WORK

In this paper a procedure with a specific setup for characterizing inertial sensors with nonlinear and dynamic effects was proposed. The procedure was deemed to be easier and less stressing to the sensors when trying to obtain nonlinear parameters and when compared to the cited literature. It was also deemed to be a more accurate way of characterizing inertial sensors when considering diverse operational conditions. The procedure was validated by using simulations limited to examples with accelerometer models. The results showed that it is indeed viable to reduce testing efforts and to add diverse operational conditions in a more accurate way to the sensor models. The consideration of dynamic effects and its automatic model selection were proposed but not yet verified.
As next steps to this work, it is necessary to verify and validate the model selection strategy. A better verification is also necessary, by using verification datasets which represent mission scenarios, instead of using only the characterization dataset. The procedure then needs to be tested on real sensors, both for accelerometers and gyroscopes. The continuation for this will be, finally, to extend this procedure to be used with enclosed IMU and Navigation Systems in order to include completely the sensor characterization in the system environmental testing.

REFERENCES

[1] "Ieee standard specification format guide and test procedure for linear single-axis, nongyroscopic accelerometers," The Institute of Electrical and Electronics Engineers (IEEE), Standard IEEE 1293:2018, Oct. 23, 2018.

[2] "Ieee standard specification format guide and test procedure for singleaxis interferometric fiber optic gyros," The Institute of Electrical and Electronics Engineers (IEEE), Standard IEEE 952:1997(R2008), Dec. 10, 2008.

[3] K. Zhang, W. Tian, and F. Qian, "A novel adaptive filter mechanism for improving the measurement accuracy of the fiber optic gyroscope in the maneuvering case," *Measurement Science and Technology*, vol. 18, no. 9, pp. 2777–2782, Sep. 2007, ISSN: 0957-0233. DOI: 10.1088/0957-0233/18/9/006

[4] C. He, C. Yang, and Z. Wang, "Fusion of finite impulse response filter and adaptive Kalman filter to suppress angle random walk of fiber optic gyroscopes," *Optical Engineering*, vol. 51, no. 12, p. 124 401, Dec. 2012, ISSN: 0091-3286. DOI: 10.1117/1.OE.51.12.124401

[5] V. Y. Senyurek, U. Baspinar, and H. S. Varol, "A modified adaptive kalman filter for fiber optic gyroscope," *Revue Roumaine des Sciences Techniques Serie Electrotechnique et Energetique*, vol. 59, no. 2, pp. 153–162, 2014, ISSN: 00354066.

[6] L. Huang, "Auto regressive moving average (ARMA) modeling method for gyro random noise using a robust kalman filter," *Sensors (Switzerland)*, vol. 15, no. 10, pp. 25 277–25 286, 2015, ISSN: 14248220. DOI: 10.3390/s151025277

[7] M. Narasimhappa, J. Nayak, M. H. Terra, and S. L. Sabat, "ARMA model based adaptive unscented fading Kalman filter for reducing drift of fiber optic gyroscope," *Sensors and Actuators, A: Physical*, vol. 251, pp. 42–51, 2016. DOI: 10.1016/j.sna.2016.09.036

[8] A. M. Kurbatov and R. A. Kurbatov, "The vibration error of the fiber-optic gyroscope rotation rate and methods of its suppression," *Journal of Communications Technology and Electronics*, vol. 58, no. 8, pp. 840–846, Aug. 2013. DOI: 10.1134/S1064226913070085

[9] Z. Gao, Y. Zhang, and Y. Zhang, "Modeling for IFOG Vibration Error Based on the Strain Distribution of Quadrupolar Fiber Coil," *Sensors*, vol. 16, no. 7, p. 1131, Jul. 2016, ISSN: 1424-8220. DOI: 10.3390/s16071131

[10] C. Shen, X. Chen, J. Yu, J. Wu, and A. N. Technology, "Random drift modeling and compensation for fiber optic gyroscope under vibration," no. 2008143, 2011.

[11] S. A. BILLINGS and Q. M. ZHU, "Rational model identification using an extended least-squares algorithm," *International Journal of Control*, vol. 54, no. 3, pp. 529–546, Sep. 1991, ISSN: 0020-7179. DOI: 10.1080/00207179108934174

[12] Q. Zhu and S. Billings, "Identification of Polynomial and Rational Narmax Models," *IFAC Proceedings Volumes*, vol. 27, no. 8, pp. 259–264, Jul. 1994. DOI: 10.1016/S1474-6670(17)47725-1

[13] L. A. Aguirre, *Introdução à Identificação de Sistemas. Técnicas Lineares e não Lineares Aplicadas a Sistemas: Teoria e Aplicação*. Editora UFMG, 2015.

[14] S. Geman, E. Bienenstock, and R. Doursat, "Neural networks and the bias/variance dilemma," *Neural Computation*, vol. 4, no. 1, pp. 1–58, 1992. DOI: 10.1162/neco.1992.4.1.1